AAS 15-624

GUIDANCE AND NAVIGATION OF A CALLISTO-IO-GANYMEDE TRIPLE FLYBY JOVIAN CAPTURE

Alan M. Didion[*] and Alfred E. Lynam[†]

Use of a triple-satellite-aided capture to enter Jovian orbit reduces insertion ΔV and provides close flyby science opportunities at three of Jupiter's four large Galilean moons. This capture can be performed while maintaining appropriate Jupiter standoff distance and setting up a suitable apojove for plotting an extended tour. This paper focuses on the guidance and navigation of such trajectories in the presence of spacecraft state errors, ephemeris errors, and maneuver execution errors. A powered-flyby trajectory correction maneuver (TCM) is added to the nominal trajectory at Callisto and the nominal Jupiter orbit insertion (JOI) maneuver is modified to both complete the capture and target the Ganymede flyby. A third TCM is employed after the flybys to act as a JOI cleanup maneuver. A Monte Carlo simulation shows that the statistical ΔV required to correct the trajectory is quite manageable.

INTRODUCTION

Satellite-aided captures involve the use of gravity-assist flybys of a satellite or satellites to reduce the orbital energy of a spacecraft such that it becomes captured by the host planet. Sometimes, the spacecraft can be captured solely by the flyby(s), but often an insertion burn is needed to complete the capture. This capture strategy can be compared to typical orbital insertion which closes the incoming hyperbola with a single retrograde burn at periapsis. Satellite-aided capture maneuvers make use of a satellite's large gravity to significantly reduce the magnitude of the insertion burn or eliminate the need for one entirely.[1,2] These maneuvers are applicable to any sizable planetary moon system, but are of particular interest in the Jupiter system wherein the four Galilean moons provide large gravity-assist potential, are in a predictable resonance pattern, and are of relevant scientific interest.[3,4,5,6] Double-, triple- and rare quadruple-satellite-aided capture opportunities have been predicted and examined by Lynam.[7,8] A preliminary navigation analysis of double and triple-satellite-aided capture trajectories was performed by Lynam and Longuski.[9] They demonstrated that trajectory correction maneuvers are needed to successfully navigate triple-satellite-aided capture trajectories. Didion and Lynam examined and targeted a particular triple-satellite-aided capture trajectory that encountered Jupiter's Galilean moons Callisto, Io and Ganymede, and included a retrograde insertion maneuver at perijove (before the Ganymede encounter).[10] This trajectory was modeled without navigation errors and was purely ballistic, except for the main impulsive perijove maneuver. It was found that the Io and especially Ganymede fly-

[*] Graduate Student, Mechanical and Aerospace Engineering, West Virginia University, ESB, Evansdale Dr., Morgantown, WV 26506.
[†] Assistant Professor, Mechanical and Aerospace Engineering, West Virginia University, ESB, Evansdale Dr., Morgantown, WV 26506.

bys were sensitive to initial conditions, and the question of navigational feasibility arose. Similar work by Patrick and Lynam examined a similar maneuver, but with a different Galilean moon encounter sequence, and more importantly, made use of low-thrust solar electric propulsion (SEP).[11]

This paper further investigates the Callisto-Io-JOI-Ganymede sequence formulated by Didion and Lynam. Through building a new, original, more flexible model written in MATLAB, the navigational limitations of the NASA General Mission Analysis Tool (GMAT) are eliminated and computation times are decreased. Moreover, access to tailored data, such as the state transition matrix (STM), is facilitated. Spacecraft position and velocity errors are modeled pseudo-randomly along with similar ephemeris knowledge errors pertaining to each Galilean moon. The insertion maneuver is given an error model according to Wagner and Goodson, which is also applied to new trajectory correction maneuvers.[12] The TCMs are used to correct the propagated pseudo-random errors, and each piece of data is carefully collected. An outer Monte Carlo repetition loop ensures that each of thousands of mission simulations are sufficiently randomized and cataloged. This data is then collated and/or averaged for detailed analysis.

METHODOLOGY

The previous GMAT model had much utility in ease of use and detailed graphics, which made it very suitable for prototyping the triple-satellite-aided capture trajectory. However, the built-in features suffered from long computational times and the difficulty in stopping the integrator to extract data, partially due to the complexity of this trajectory. It was decided that a MATLAB model, built in-house and starting from nothing, would be more adaptable and accessible. With this new model, pseudo-random errors could be injected at specific times and the state transition error matrix (STM) could be carried and used to target TCMs and correct the trajectory.

System Modeling in MATLAB

A model was built in MATLAB which made use of ode113 differential equation solver to integrate the seven-body dynamical system through time. In Jupiter-centered coordinates, the four Galilean moons and the sun propagated according to ephemeris checks for each time step. The four moons, the sun, and Jupiter form the gravitational model, with a negligible-mass spacecraft as the seventh body. The spacecraft began at the initial state as previously determined by Didion and Lynam in the GMAT model, as detailed below in Jupiter-centered coordinates.

Table 1: Spacecraft Initial State, Jupiter-Centered Ecliptic J2000[10]

Position [km]		
x	y	z
-4568345.274	1030.943	-60834.882
Velocity [km/s]		
u	v	w
9.248	-1.868	0.064

The model is propagated using the 3-body equations of motion as described by Vallado, which are adjusted for seven bodies.[13] This is done simply by adding more terms for each gravitational source and causes negligible additional complexity because it assumes the spacecraft has no gravity of its own and the celestial bodies are "on rails", or do no experience dynamical forces; they only move according to the ephemeris predictions.

$$\ddot{\vec{r}}_{J-SC} = -\frac{\mu_J \vec{r}_{J-SC}}{\left\|\vec{r}_{J-SC}\right\|^3} + \sum_{i=1}^{5} \mu_i \left(\frac{\vec{r}_{SC-i}}{\left\|\vec{r}_{SC-i}\right\|^3} - \frac{\vec{r}_{J-i}}{\left\|\vec{r}_{J-i}\right\|^3} \right) \quad (1)$$

Where "SC" denotes a quantity pertaining to the spacecraft, "J" for Jupiter, and "i" for each third body; e.g.: terms such as "SC-i" denote quantities pertaining to a third body in relation to the spacecraft. This equation describes how the spacecraft accelerates in response to the gravity of Jupiter and each of the "third bodies". In this case, the term for a third body was repeated a total of five times using the parameters for the sun and each of the four Galilean moons respectively. This served as the differential equation for the ode113 integrator, solving for the trajectory of the spacecraft with time as it traveled through the system.

Each integration step propagated the state of the spacecraft (six elements) as well as a STM which incorporated the errors for each body, allowing for easy propagation of inserted errors as described in the next section. Because the ode113 function inputs and outputs a row vector, the STM had to be repeatedly flattened and reshaped in order to extract the necessary information. In row form, the vector handled by ode113 was a 1x330 row, which was reduced to 1x324 after separating the STM from the first six entries that represent the spacecraft state. This could then be easily reshaped into the 18x18 STM, as it was used in the following section to handle error propagation.

The trajectory was split into mission "phases": branches between specific points of interest at which the integration pauses. In the scheme used here, the pauses represented an instant in which took place several simultaneous, instantaneous processes. Pauses were enforced by an "events" function inserted into the ode113 options, and took place at critical points such as periapsides, as follows: initial state, Callisto periapsis, Io periapsis, Jupiter periapsis, Ganymede periapsis, arbitrary point outside Ganymede's influence, Jupiter apoapsis. At each pause, the spacecraft gained instantaneous knowledge of its state and the bodies around it, which it used to target TCMs and correct the next phase of the trajectory. Once targeted, the TCMs are instantaneously executed before the end of the pause. All of these pieces of knowledge, as well as the TCM execution itself, were subject to error, as is explained in the following sections.

Insertion of State Errors

At each pause, appropriate state errors were determined for the situation before integration resumed; these represent errors in the spacecraft position and velocity as well as ephemeris errors for the position of each Galilean moon. The errors were implemented using a call of "randn" for each value each time, multiplying the randn result by a "reasonable" standard deviation value for each error, as detailed below in Table 2. We assume that radiometric navigation could provide sufficient trajectory knowledge to reduce the initial state uncertainty to that level. The errors on the moons positions represent the uncertainty of our present ephemeris knowledge of the Galilean moons.

Table 2: Standard Deviations for State Errors

	Position [km]			Velocity [mm/s]		
SC	δx	δy	δz	δu	δv	δw
Initial State	1.0	1.0	1.0	1.0	1.0	1.0
Other	0.1	0.1	0.1	1.0	1.0	1.0
Moons						
Departure	0.1	0.1	0.1			
Arrival	5.0	10.0	5.0			

For each pause, there were six errors applied to the spacecraft state, and three position errors applied to each applicable moon. The spacecraft state error was assumed to be large at the initial state and an order of magnitude smaller at all other pauses. The values in the lower half of Table 2 detail the smaller errors at the moon currently being departed and larger errors for the next to be encountered, e.g.: at the pause at Callisto periapsis, there is a small error on Callisto's position and a large error on Io's position. Likewise, the pause at Ganymede periapsis experienced small

error in Ganymede's position, but no "arrival" error, because the next pause point is in open Jovian space. Once a vector of "reasonable" errors was determined, it was multiplied by the propagated state error transition matrix from the previous integration and the spacecraft state was updated to reflect the error. This new state was the state plotted and used for the next integration.

B-plane Targeting & TCMs

At Callisto periapsis, a TCM was used to ensure the next arrival at Io was in the required area of the Io B-plane in order to achieve the desired flyby. Likewise, the composite JOI maneuver was targeted to properly intercept Ganymede's B-plane. To achieve this, the Callisto periapsis pause and the JOI pause featured B-plane targeting loops which would apply a "guess" TCM, propagate until arrival, calculate the B-plane, and repeat with a new TCM depending on an objective function until agreement with desired values was reached. The objective function logic is explained below, given the B-plane dot products and derivatives from geometry, where Φ is the STM as previously described and X is the spacecraft state.

$$F = \begin{bmatrix} B \cdot R_{act} - B \cdot R_{nom} \\ B \cdot T_{act} - B \cdot T_{nom} \end{bmatrix} \tag{2}$$

$$\frac{dX}{du} = \varphi(1{:}\,6,4), \frac{dX}{dv} = \varphi(1{:}\,6,5), \frac{dX}{dw} = \varphi(1{:}\,6,6) \tag{3}$$

$$\mathrm{DF} = \begin{bmatrix} \frac{d(B\cdot R)}{dX} * \frac{dX}{du} & \frac{d(B\cdot R)}{dX} * \frac{dX}{dv} & \frac{d(B\cdot R)}{dX} * \frac{dX}{dw} \\ \frac{d(B\cdot T)}{dX} * \frac{dX}{du} & \frac{d(B\cdot T)}{dX} * \frac{dX}{dv} & \frac{d(B\cdot T)}{dX} * \frac{dX}{dw} \end{bmatrix} \tag{4}$$

$$TCM_1 = TCM_0 - DF'/(DF' * DF) * F \tag{5}$$

In Equation 2, an objective function F was set up, representing the difference between the desired, nominal (nom) B-plane dot products and the actual values achieved. This objective function ultimately determined when the target was reached and the targeting loop could end. Equation 3 represented state derivatives as extracted from the STM, which were needed to take the derivative of F, as calculated in Equation 4. Finally in Equation 5, the TCM was updated with a new "guess", according to a function of the derivative of the objective function with the change in TCM components. This logic then repeated, integrating from the same state with the new TCM, calculating the B-plane parameters each time until both values of the F matrix were lower than an applied tolerance; in this case, the tolerance used was one meter. This entire process served to both target the necessary ideal TCMs and to correct position and velocity error as inserted previously. However, these maneuvers were still subject to error themselves, as described in the next section.

Maneuver Execution Error

Maneuver execution error was applied onto each TCM as well as the JOI maneuver and was based on the maneuver error model analyzed by Wagner and Goodson.[12] This model provides proportional and fixed error magnitudes describing Cassini's main engine assembly (MEA) and reaction control system (RCS) propulsion methods. The error for TCMs 1 and 2 were modeled using the RCS values, while the JOI composite maneuver was modeled using the MEA values as shown in Table 3. These values represent the standard deviation values and errors are applied by multiplying a "randn" call by the model equation and adding them vectorially onto the ideal maneuvers. The equations are also given below, with σ_1 being the fixed values, σ_2 being the proportional values, and y being the magnitude of the nominal maneuver.

Table 3: Maneuver Execution Error Model[12]

		MEA	RCS
Magnitude	Proportional [%]	0.02	1.2
	Fixed [mm/s]	5.0	0.8
Pointing (per axis)	Proportional [mrad]	0.6	5.5
	Fixed[mm/s]	3.0	0.0

$$d\Delta V = randn * \sqrt{{\sigma_1}^2 + y^2{\sigma_2}^2} \tag{6}$$

This leads to the following set of equations, with "mag", "point1", and "point2" forming an orthogonal set representing the magnitude error, in the direction of the nominal maneuver, and two pointing errors, oriented at right angles to the maneuver direction, $\Delta\hat{V}$. These equations are used similarly when calculating the TCM errors with the RCS values, wherein the "y_{JOI}" would be replaced by "y_{TCM}", the magnitude of the nominal TCM.

$$d\Delta V_{mag_{MEA}} = randn * \sqrt{{\sigma_{1_{mag_{MEA}}}}^2 + {y_{JOI}}^2{\sigma_{2_{mag_{MEA}}}}^2} * \Delta\hat{V} \tag{7}$$

$$d\Delta V_{point1_{MEA}} = randn * \sqrt{{\sigma_{1_{point_{MEA}}}}^2 + {y_{JOI}}^2{\sigma_{2_{point_{MEA}}}}^2} * \Delta\hat{V}_{p1} \tag{8}$$

$$d\Delta V_{point2_{MEA}} = randn * \sqrt{{\sigma_{1_{point_{MEA}}}}^2 + {y_{JOI}}^2{\sigma_{2_{point_{MEA}}}}^2} * \Delta\hat{V}_{p2} \tag{9}$$

$$d\Delta V_{MEA} = d\Delta V_{mag_{MEA}} + d\Delta V_{point1_{MEA}} + d\Delta V_{point2_{MEA}} \tag{10}$$

In these equations, the unit vectors can be described by the below relations, where $\hat{z}$ is the vertical direction unit vector.

$$\Delta\hat{V} = \frac{\Delta V}{\|\Delta V\|}, \quad \Delta\hat{V}_{p1} = \Delta\hat{V} \times \hat{z}, \quad \Delta\hat{V}_{p2} = \Delta\hat{V} \times \Delta\hat{V}_{p1} \tag{11}$$

The result of Equation 10 was then added onto the nominal maneuver and propagation continued. This occurred using the appropriate values from Table 3 **Error! Reference source not found.**for each of the two TCMs and for the adjusted JOI composite maneuver.

Statistical Modeling via Monte Carlo Simulation

In order to determine the stochastic robustness of this mission profile and ultimately determine its average sensitivity to reasonable perturbations, a Monte Carlo simulation scheme was developed to repeat the MATLAB script several thousand times, each with new pseudo-random perturbations. This scheme was implemented by creating a simple frame script which randomizes the "randstream" seed variable based on the current clock time and the mt19937ar algorithm, ensuring that each repeated run receives legitimately different pseudo-random values for continued calls of "randn". Without this measure, it would be unclear whether the randstream was being reused for continued runs. The repetition script set up a while loop which ran until a set time of day (usually overnight), repeatedly running the simulation function and appending a vector of mission data onto a large array. This large array was then saved into an excel sheet for statistical post-processing.

RESULTS

This section discusses the outcome of performing the triple-satellite-aided capture sequence in the complete Jovian system model in MATLAB. First, data is presented to verify that without perturbations, a nominal trajectory through this sequence matched, within reasonable tolerance,

the GMAT trajectory of the same initial conditions and given maneuvers. Second, the results of the Monte Carlo repetition of the script, with pseudo-random perturbations injected at the appropriate points, are presented and discussed. Data on the statistical distributions of physical trajectory parameters are presented, with graphical representations of each of the individual moons' flyby B-planes.

Verification of the MATLAB Model & Nominal Characteristics

The new MATLAB model was verified for accuracy against the previously used GMAT model before proceeding. This was done by giving the MATLAB model the full set of initial spacecraft conditions, the set JOI magnitude, and the ephemeris epoch used in the GMAT model. The spacecraft was then allowed to freely propagate through the nominal trajectory without any perturbations, targeting, or trajectory correction. At the end, the position of the spacecraft during flybys is compared to the GMAT model. The radial error at Callisto was 0.10%, which when left to ballistically propagate without errors or correction led to a 2.67% radial error at Ganymede closest approach. The final period was 295.271 days, within 5 days of the 300 day target. This error was deemed acceptable, and analysis continued with the new MATLAB model. Below, in Table 4, are the "expected" nominal trajectory parameters for the mission (from GMAT), against which will later be compared the average values of the Monte Carlo simulation.

Table 4: Expected Nominal Parameters from GMAT Model

Callisto Alt.	505.0	[km]
Io Alt.	282.0	[km]
Ganymede Alt.	98.5	[km]
Perijove Radius	3.3	[RJ]
JOI	253.0	[m/s]
Final Period	300.0	[day]

Monte Carlo Statistical Characteristics

Using the Monte Carlo repetition frame script previously described, a total of approximately 2500 mission runs were completed and all relevant values were catalogued. Brief post-processing of the data in Excel confirmed that of the 2500 runs, not a single case resulted in failure, i.e., no run failed to converge, and no trajectory intersected the surface of a moon, used excessive ΔV, or failed to achieve the desired 300 day final orbital period. Furthermore, the data collected was analyzed to extract the statistical properties of each individual quantity of interest, including the minimum, maximum, range, and standard deviation of each flyby radius/altitude, B-plane parameters, final period, and TCM and JOI magnitudes. Below in Figure 1 is an example trajectory, a single run through the triple-satellite-aided capture sequence showing the locations of each of the flybys at the time of closest approach, apojove is not shown. All integration pauses are marked with a X, moons with a circle, and Jupiter with a star. Note the post-Ganymede TCM pause that does not coincide with a flyby, and the JOI pause at perijove. On this scale, all of the Monte Carlo runs would look exactly like Figure 1.

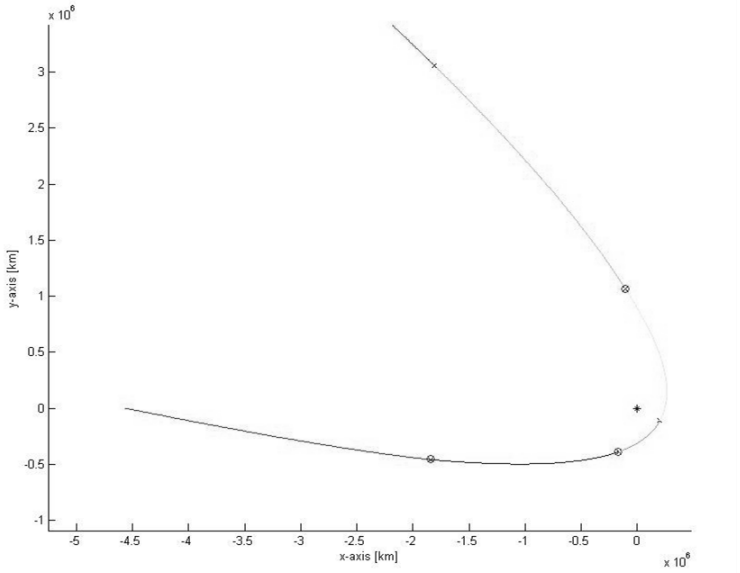

Figure 1: Example Callisto-Io-JOI-Ganymede Trajectory, Jupiter-Centered Coordinates

Because the initial state is subject to errors in position and velocity of Jupiter, Callisto, and the spacecraft, and it does not receive a TCM before the ballistic approach to Callisto, the Callisto flyby experiences the greatest spread in B-plane parameter error. However, the errors experienced are still relatively small, and the Callisto periapsis TCM is performed afterwards, beginning the navigation and ensuring smaller errors for the subsequent mission phases. Below, Table 5 details the statistical properties of the Callisto flyby, while Figure 2 gives a graphical scatter plot showing the B-plane intersection point spread for the 2500 script repetitions.

Table 5: Callisto Flyby Statistical Properties

	Rp	Altp	BdotR	BdotT	B Angle
Average	2918.11	507.81	-2.03	2962.49	-0.04
Min.	2914.56	504.26	-5.26	2958.94	-0.10
Max	2921.80	511.50	1.22	2966.18	0.02
Range	7.25	7.25	6.48	7.24	0.13
Std. Dev.	1.00		0.95	1.00	0.02
	[km]	[km]	[km]	[km]	[deg]

It is important to note the scale of these scatter plots, which is too small to warrant display relative to the surfaces of the moons. The scale has been chosen instead to adequately show the scatter pattern. Also shown are inner and outer probability error ellipses corresponding to 1-σ (68.3%) and 3-σ (99.7%) respectively.

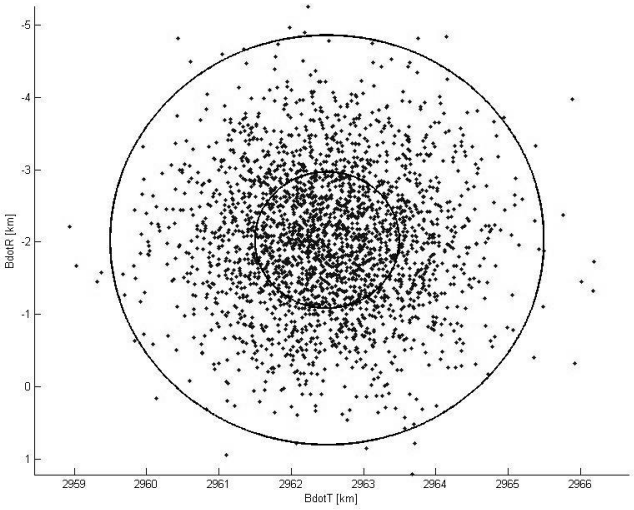

Figure 2: Callisto B-plane Scatter, with 1-σ and 3-σ Error Ellipses

Note that the range in Callisto flyby altitude is still only 7.25 km, with a very safe minimum altitude of 504.26 km. Furthermore, the B-plane angle achieves an average of -0.04 deg, very close to the desired 0 deg planar flyby. Similarly, the Io flyby is analyzed to reveal its statistical distribution and B-plane spread. Table 6 and Figure 3 below detail these results.

Table 6: Io Flyby Statistical Properties

	Rp	Altp	BdotR	BdotT	B Angle
Average	2112.42	290.82	-964.63	1902.30	-26.89
Min.	2109.67	288.07	-967.36	1899.38	-26.95
Max	2115.19	293.59	-962.35	1904.49	-26.83
Range	5.53	5.53	5.01	5.11	0.13
Std. Dev.	0.40		0.37	0.41	0.01
	[km]	[km]	[km]	[km]	[deg]

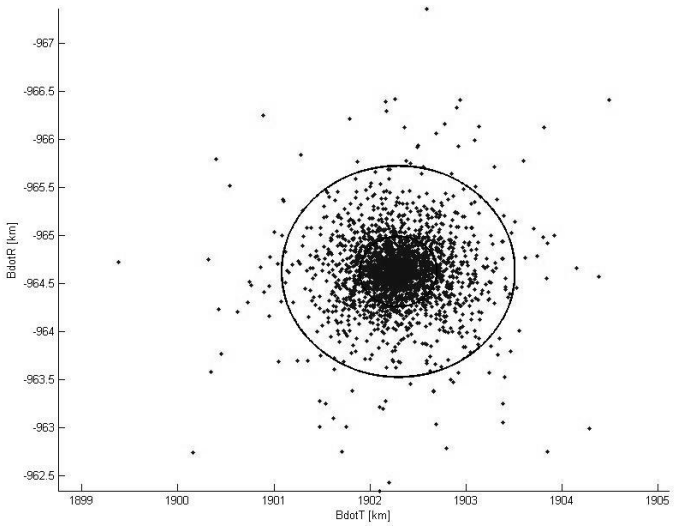

Figure 3: Io B-plane Scatter, with 1-σ and 3-σ Error Ellipses

Because the Callisto periapsis TCM serves to target the Io flyby, the spread here is much more controlled, with a range of 5.53 km and a safe minimum altitude of 288.07 km. Note that the Callisto periapsis TCM targets a specific Io B-plane angle in order to reach a suitable inclination to reach Ganymede. The angle here is very consistent around the average of -26.89 deg with a range of only 0.13 deg. Again, after JOI and its associated adjustment, which is treated like a TCM, a similar set of data is presented for the Ganymede flyby below in Table 7 and Figure 4.

Table 7: Ganymede Flyby Statistical Properties

	Rp	Altp	BdotR	BdotT	B Angle
Average	2729.68	98.48	512.52	-2731.33	169.37
Min.	2721.01	89.81	511.23	-2740.05	169.33
Max	2738.17	106.97	514.08	-2722.64	169.42
Range	17.16	17.16	2.84	17.41	0.09
Std. Dev.	2.66		0.42	2.72	0.01
	[km]	[km]	[km]	[km]	[deg]

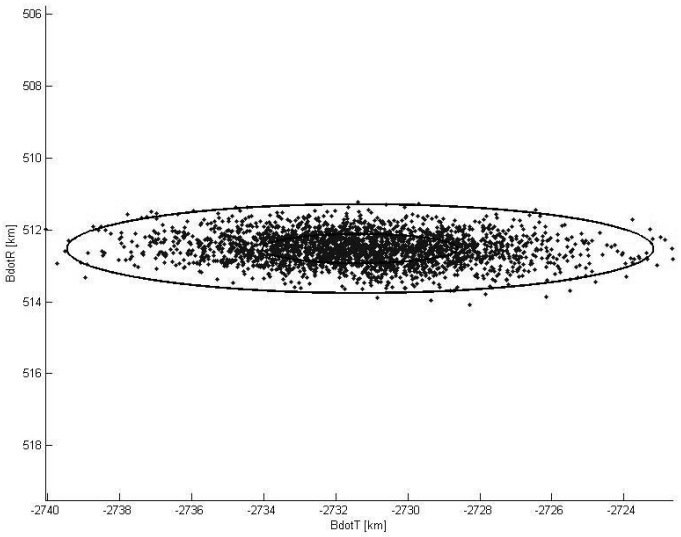

Figure 4: Ganymede B-plane Scatter, with 1-σ and 3-σ Error Ellipses

The Ganymede flyby spread is relatively controlled in BdotR, but varies a relatively large amount in BdotT, with ranges of 2.84 km and 17.41 km respectively. This is, however, not an issue because the Ganymede flyby is not critical for targeting subsequent flybys like the previous ones. Because the altitude does not vary significantly, the flyby is successful as it receives sizable gravity assist without approaching dangerously close; and the following TCM 2 can easily correct these errors to target the appropriate apojove. TCM 2 is essentially a JOI cleanup maneuver, so it is not required to safely navigate the flybys. However, the subsequent Jupiter satellite tour would require it to efficiently target the first flyby after capture.

The script recorded all of the components for each maneuver, and through post-processing the statistical properties were extracted for each component. Additionally, the mission ΔV was recorded and analyzed similarly. The reduced statistical maneuver data can be examined below in Table 8.

Table 8: Statistical Maneuver Data [m/s]

	TCM 1 (Callisto periapsis)			**Nominal JOI**			**JOI Adjustment**		
	ΔVx	**ΔVy**	**ΔVz**	**ΔVx**	**ΔVy**	**ΔVz**	**ΔVx**	**ΔVy**	**ΔVz**
Average	0.000	0.000	0.009	-122.615	-221.027	-8.767	-1.178	-0.378	2.666
Min.	-0.837	-0.198	-1.246	-122.737	-221.092	-8.772	-23.506	-4.787	1.418
Max.	0.928	0.177	1.242	-122.497	-220.960	-8.762	21.191	4.055	4.320
Range	1.765	0.375	2.488	0.240	0.133	0.010	44.697	8.842	2.902
Std. Dev.	0.271	0.059	0.347	0.037	0.020	0.001	6.788	1.347	0.400
	TCM 2 (post-Ganymede)			**Apojove Period Match**			**Mission ΔV**		
	ΔVx	**ΔVy**	**ΔVz**	**ΔVx**	**ΔVy**	**ΔVz**	**Magnitude**		
Average	-0.026	0.032	0.001	0.000	-0.001	0.000	272.442		
Min.	-23.850	-69.106	-2.863	-1.217	-1.718	-0.102	253.982		
Max.	21.028	69.587	2.564	1.324	1.813	0.108	345.523		
Range	44.878	138.693	5.427	2.541	3.531	0.211	91.542		
Std. Dev.	6.771	20.941	0.862	0.387	0.536	0.034	14.344		

This table details the average, minimum, etc. of each component of each maneuver in m/s. It is important to note that these are the bounds of each component, and do not correspond to a partic-

ular maneuver instance. A histogram showing mission ΔV magnitude probability distribution can be examined in Figure 5.

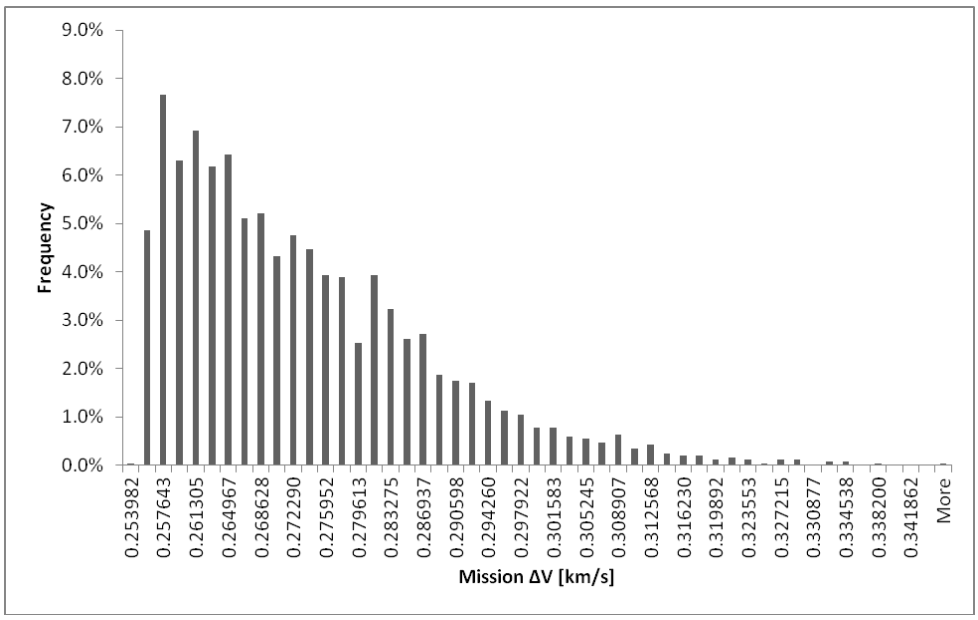

Figure 5: Mission ΔV Histogram

As is shown, the mission ΔV probability distribution is heavily skewed toward the low end, but covers a sizable range, from 253.982 m/s to the 99th percentile value of 317.619 m/s (with a few outliers above that value). However, the average is 272.442 m/s, the median is 269.132 m/s, and the probability distribution peaks at an expected mission ΔV value of 257.643 m/s, representing nearly 8% of all mission runs, 197 runs. This further demonstrates the higher probability toward less ΔV, with the extreme maximum having a very rare chance of occurrence when unfavorable perturbations combined, resulting in only six of the 2500 runs requiring a ΔV of more than 330 m/s. Furthermore, because the ideal post-Ganymede TCM experiences no execution error, it had no issue achieving 295.271 day period of the nominal MATLAB trajectory, with a range and standard deviation on the order of the machine's precision due to its deterministic behavior.

CONCLUSION

As a general measure of success, the Monte Carlo simulation experienced no fatal script errors and no instances of a sub-surface flyby. The statistical properties of the mission ΔV requirements are consistent and favorable, demonstrating that the mission is feasibly navigable given reasonable errors. Perturbations do not in any case cause extreme course deviations that cannot be corrected with modest trajectory corrections. As will be discussed in the following sections, the results fall within expected boundaries and represent an efficient, desirable mission design for Jovian capture which can be used for missions with various means and ends. The method employed is rigorous and adjustable, statistically stable and theoretically sound.

Delta-v Comparison

The flyby sequence examined here was a triple-satellite-aided capture with a perijove radius of approximately 3.3 RJ, yielding a median mission ΔV of 269.132 m/s and median adjusted JOI magnitude of 253.686 m/s. This approximately fits in the preliminary navigation findings of

Lynam and Longuski, as shown by their representative data shown in Table 9, which claimed a best-case triple-flyby JOI of 245 m/s with a perijove of 3 RJ.

Table 9: JOI ΔV [m/s] for best Jupiter Capture at various RJ[9]

Flyby Sequences	5 RJ	4 RJ	3 RJ	2 RJ	1 RJ
Unaided	825	735	641	524	371
Best Single	556	526	483	416	308
Best Double	330	340	333	299	228
Best Triple	202	232	245	234	190
Best Quad	N/A	N/A	N/A	175	160

These data further suggest that triple-satellite-aided captures may arguably provide the best opportunities for entry into the Jovian system. This is partially due to the non-existence of quadruple flyby sequences with reasonable perijove radii; a perijove radius of less than 3 RJ would experience intense radiation from Jupiter, making only the first three columns of data worth considering. Of these, the triple-flyby sequence clearly provides substantial ΔV reduction over other methods of capture.

Adaptability

Because the MATLAB model is all original script, written functionally and with an adaptive step size ode113 integrator, it can be easily modified to similarly examine different flyby sequences and even use low-thrust SEP. Such work has been examined in other existing software packages by Patrick and Lynam.[11] This method allows for alteration of all spacecraft initial conditions, allowing for various modes of interplanetary intercept, rather than the simple near-Hohmann transfer employed to reach the initial state in this mission profile. By altering the interplanetary course, flyby encounter order, propulsion method and flyby safety margins, the capture could be further optimized for absolute minimal ΔV or for a particular science schedule. This being said, further investigation would be required in order to determine if SEP would indeed be capable of performing the necessary corrections under the influence of the applied errors.

ACKNOWLEDGEMENTS

The authors would like to thank the AAS and AIAA as well as West Virginia University and the NASA West Virginia Space Grant Consortium for their support.

REFERENCES

[1] Longman, R. W., "Gravity Assist from Jupiter's Moons for Jupiter-Orbiting Space Missions," *The RAND Corp.*, Santa Monica, CA, 1968.

[2] Broucke, R. A., "The Celestial Mechanics of Gravity Assist," *Proceedings of the AIAA/AAS Astrodynamics Specialist Conference*, AIAA Paper 88-4220-CP, Minneapolis, MN, August 1988.

[3] Lynam, A. E., Kloster, K. W., and Longuski, J. M., "Multiple-Satellite-Aided-Capture Trajectories at Jupiter Using the Laplace Resonance," *Celestial Mechanics and Dynamical Astronomy*, Vol. 109, No. 1, 2011, pp. 59-84.

[4] Laplace, P. S., *The System of the World*, W. Flint, London, 1809.

[5] Strom, R. G., Terrile, R. J., Hansen, C., Masursky, H., "Volcanic eruption plumes on Io," *Nature*, Vol. 280, August 1979, pp. 733-736.

[6] Plainaki, C., Milillo, A., Massetti, S., Mura, A., Jia, X., Orsini, S., Mangano, V., De Angelis, E., Rispoli, R., "The H2O and O2 exospheres of Ganymede: The result of a complex interaction between the jovian magnetospheric ions and the icy moon," *Icarus*, Vol. 245, January 2015, pp. 306-319.

[7] Lynam, A. E., "Broad-search Algorithms for the Spacecraft Trajectory Design of Callisto-Ganymede-Io Triple Flyby Sequences from 2024 to 2040, Part 1: Heuristic Pruning of the Search Space," *Acta Astronautica*, Vol. 94, No. 1, Jan.-Feb. 2014, pp. 246-252.

[8] Lynam, A. E., "Broad-search Algorithms for the Spacecraft Trajectory Design of Callisto-Ganymede-Io Triple Flyby Sequences from 2024 to 2040, Part 2: Lambert Pathfinding and Trajectory Solutions," *Acta Astronautica*, Vol. 94, No.1, Jan.-Feb. 2014, pp. 253-261.

[9] Lynam, A. E., and Longuski, J. M., "Preliminary Analysis for the Navigation of Multiple-satellite-aided Capture Sequences at Jupiter," *Acta Astronautica*, Vol. 79, No. 5, 2012, pp. 33-43.

[10] Didion, A. M., and Lynam, A. E., "Impulsive Trajectories from Earth to Callisto-Io-Ganymede Triple Flyby Jovian Capture," *AAS/AIAA Astrodynamics Specialist Conference*, AIAA Paper 2014-4106, San Diego, California, August 2014.

[11] Patrick, S. K., and Lynam, A. E., "Optimal SEP Trajectories from Earth to Jupiter with Triple Flyby Capture," *AAS/AIAA Astrodynamics Specialist Conference*, AIAA Paper 2014-4218, San Diego, CA, August 2014.

[12] Wagner, S. V., and Goodson, T. D., "Execution-Error Modeling and Analysis of the Cassini-Huygens Spacecraft Through 2007," *Proceedings of the AAS/AIAA Space Flight Mechanics Meeting*, AAS Paper 08-113, Galveston, TX, January 2008.

[13] Vallado, D. A., McClain, W.D., *Fundamentals of Astrodynamics and Applications*, Netherlands: Springer Science and Business Media, 2nd ed., 2001